water

MDPI

Article

Spatial Estimates of Flood Damage and Risk Are Influenced by the Underpinning DEM Resolution: A Case Study in Kuala Lumpur, Malaysia

Eva Fatdillah [1], Balqis M. Rehan [1,*], Ponnambalam Rameshwaran [2], Victoria A. Bell [2], Zed Zulkafli [1], Badronnisa Yusuf [1] and Paul Sayers [3]

[1] Faculty of Engineering, Universiti Putra Malaysia, Seri Kembangan 43400, Selangor, Malaysia; evalailatunnisa15@gmail.com (E.F.); zeddiyana@upm.edu.my (Z.Z.); nisa@upm.edu.my (B.Y.)
[2] UK Centre for Ecology and Hydrology, Wallingford OX10 8BB, UK; ponr@ceh.ac.uk (P.R.); vib@ceh.ac.uk (V.A.B.)
[3] Sayers and Partners LLP, 24a High Street, Watlington OX49 5PY, UK; paul.sayers@sayersandpartners.co.uk
* Correspondence: balqis@upm.edu.my

Abstract: The sensitivity of simulated flood depth and area to DEM resolution are acknowledged, but their effects on flood damage and risk estimates are less well understood. This study sought to analyse the relative benefits of using global DEMs of different resolution sizes, 5 m AW3D Standard, 12.5 m ALOS PALSAR and 30 m SRTM, to simulate flood inundation, damage and risk. The HEC-RAS 2D model was adopted for flood simulations, and the Toba River in the Klang River Basin in Malaysia was chosen for the case study. Simulated inundation areas from AW3D coincide the most with reported flooded areas, but the coarser-resolution DEMs did capture some of the reported flooded areas. The inundation area increased as the resolution got finer. As a result, AW3D returned almost double flood damage and risk estimates compared to ALOS PALSAR, and almost quadruple compared to SRTM for building-level damage and risk analysis. The findings indicate that a finer-resolution DEM improves inundation modelling and could provide greater flood damage and risk estimates compared to a coarser DEM. However, DEMs of coarser resolution remain useful in data-scarce regions or for large-scale assessments in efforts to manage flood risk.

Keywords: hydraulic modelling; digital elevation model; flood damage; flood risk

Citation: Fatdillah, E.; Rehan, B.M.; Rameshwaran, P.; Bell, V.A.; Zulkafli, Z.; Yusuf, B.; Sayers, P. Spatial Estimates of Flood Damage and Risk Are Influenced by the Underpinning DEM Resolution: A Case Study in Kuala Lumpur, Malaysia. *Water* **2022**, *14*, 2208. https://doi.org/10.3390/w14142208

Academic Editor: Chang Huang

Received: 11 June 2022
Accepted: 4 July 2022
Published: 13 July 2022

1. Introduction

Floods have caused devastating impacts and losses to the world community. Climate-related disasters have constituted up to 91% of the 7255 disaster events that were recorded between 1998 and 2017, and floods accounted for 43% of all tallied disasters, making them the most common type [1]. Furthermore, the global exposure to floods is likely to increase by three times by 2050; the largest absolute changes can be expected in North America and Asia [2]. Future flood events may not be preventable due to their uncertain nature and considering exacerbation from climate change. Jha et al. [3] summarized that climate change significantly affects flood risk in four ways: (i) rise of sea water level, resulting in more coastal flooding; (ii) alteration of local rainfall patterns leading to more riverine flooding and flash flooding; (iii) changes in frequency and duration of drought, causing groundwater extraction and land subsidence; and (iv) increase in frequency of storm occurrence, leading to more frequent storm surges. Moreover, population growth, increasing urbanization and infrastructure decay can be attributed as factors contributing to the trend of increasing in economic losses due to flooding [4]. However, the risk of flooding can be reduced through the implementation of strategies that are developed with assistance from simulations of probable flood inundation depths, area and damage. Not only that, statistical validation techniques can be used to provide a flood risk index on a municipal scale using different

sources of municipal-level data [5]. For the regional scale, Aroca-Jiménez et al. [6] presented the construction of an integrated socio-economic vulnerability index (ISEVI) that considers all vulnerability components and social and economic dimensions.

A digital elevation model (DEM) that provides terrain information is intrinsic to flood inundation modelling, damage and risk analysis. DEM data can be obtained from various data sources: (i) contour maps through ground surveys; (ii) light detection and ranging (LiDAR) through airborne laser scanning; and (iii) remotely sensed data, such as those from Cartosat-1, ASTER (Advanced Spaceborne Thermal Emission and Reflection Radiometer) and Shuttle Radar Topography Mission (SRTM) [7]. Recently, there has been growing technology for unmanned aerial vehicles (UAV), popularly called 'drones', to collect large amount of elevation data [8]. One of the main characteristics of DEM is its resolution, which inevitably influences flood inundation simulations [7,9]. The most preferred DEM for flood studies is LiDAR due to its high accuracy. However, a high-resolution DEM such as LiDAR is often unavailable due to its high production cost, and to some extent because of privacy and safety reasons. These limitations have steered flood studies towards using global DEMs that are accessible and relatively affordable. Furthermore, global DEMs have proven to be useful in flood inundation and risk analysis, especially for data-scarce regions and large-scale assessments.

Acknowledging that DEMs of different resolutions could lead to disparities of inundation simulation, various studies were undertaken to investigate the effects of DEM resolution. The uncertainty caused by DEM resolutions in inundation model output is typically evaluated using reference cases, such as those from observed data or simulations with the highest possible resolution available (e.g., LiDAR DEM). Errors in flood inundation are generally found to be much greater from a low-resolution DEM than a high-resolution DEM. For example, McClean et al. [10] found that flood inundation is overestimated by 2 to 3 times when using global DEM of coarse resolution compared to LiDAR. Meanwhile, Bhuyian and Kalyanapu [11] also demonstrated that the uncertainty in flood consequence (i.e., number of structures affected) depends on the DEM type and resolution. These show that the DEM properties are critical in determining the risk of flooding.

Despite the various studies that have investigated the effects of DEM types and resolutions to flood inundation, not many studies have attempted to quantify the sensitivity caused by the different DEM resolutions in the inundation modelling to flood damage and risk. The valuation task is a challenge if historical information and datasets are limited [12]. With the absence of information, the challenge remains in efforts to validate flood risk models as a whole [13]. To offset the data unavailability, flood risks with inherent errors in the inundation modelling can be analysed in terms of their sensitivity to changes in the DEM type and resolutions [14]. In a developing country that has the same tropical weather, Costa Rica, where baseline information is lacking, Quesada-Román et al. [15] presented a technique for regional flood risk assessments in large-scale catchments. Other than that, the hydrometeorological risk assessment based on population census minimum geostatistical units to depict a spatially distributed risk matrix is a methodology with which to assess flash flood impact due to a hurricane [16]. Pinos et al. [17] proposed an open-access tool using accessible data at the municipality level to assess economic flood losses in urban and agriculture areas.

This study sought to examine the sensitivity of flood inundation characteristics (i.e., depth and flooded area) to flood damage and risk arising from different DEM resolutions. Three global DEM data products were used: SRTM (with a 30 m resolution), ALOS PALSAR (with a 12.5 m resolution) and AW3D Standard (with a 5 m resolution). The Toba River, located in Kuala Lumpur, Malaysia, which frequently experiences fluvial flooding, was chosen for the investigation. The Toba River does not appear in the global topographic data because of its small width; hence, a pre-processing step was undertaken to modify the riverbed level and width consistently across all considered DEMs following available survey information. The following sections are as follows: Section 2 explains the study

area, Section 3 describes the developed methodology and data used, Section 4 presents and discusses the results, and Section 5 concludes the study.

2. Study Area

Lowland areas in Kuala Lumpur are often hit by floods, mostly initiated by high intensity of short-duration rainfall (i.e., [18]). The Toba Catchment, a sub-basin of the greater Klang River basin located upstream of Kuala Lumpur, Malaysia, was selected for the case study. This catchment is located northwest of Kuala Lumpur (Figure 1a) and lies between the latitudes of 3°9′45″ N to 3°12′00″ N and longitudes 101°38′00″ E and 101°42′00″ E. It has a river length of 2.56 km, an average river width of 7.32 m, and a catchment area of 8.47 km^2. The headwaters of the Toba River start in the southwest of the catchment and join the Keroh River at the downstream end. A review of flood reports and consultations with stakeholders from the Kuala Lumpur City Hall (DBKL) has led to the selection of the Toba Catchment. Mainly, the selection focuses on a basin that is prone to fluvial flooding. From the flood reports, multiple flood occurrences have been recorded along the Toba River from 2009 to 2020, which are summarized in Table 1. The range of flood depths on roads and community areas was between 0.3 and 1.0 m [19]. The reported flood depths are based on the approximations right after flood events and are bound to have inaccuracies. The data are here to provide prior insight into areas that are prone to flooding and the intensity of the events, yet the information cannot accurately be referred to given that the data are not absolute.

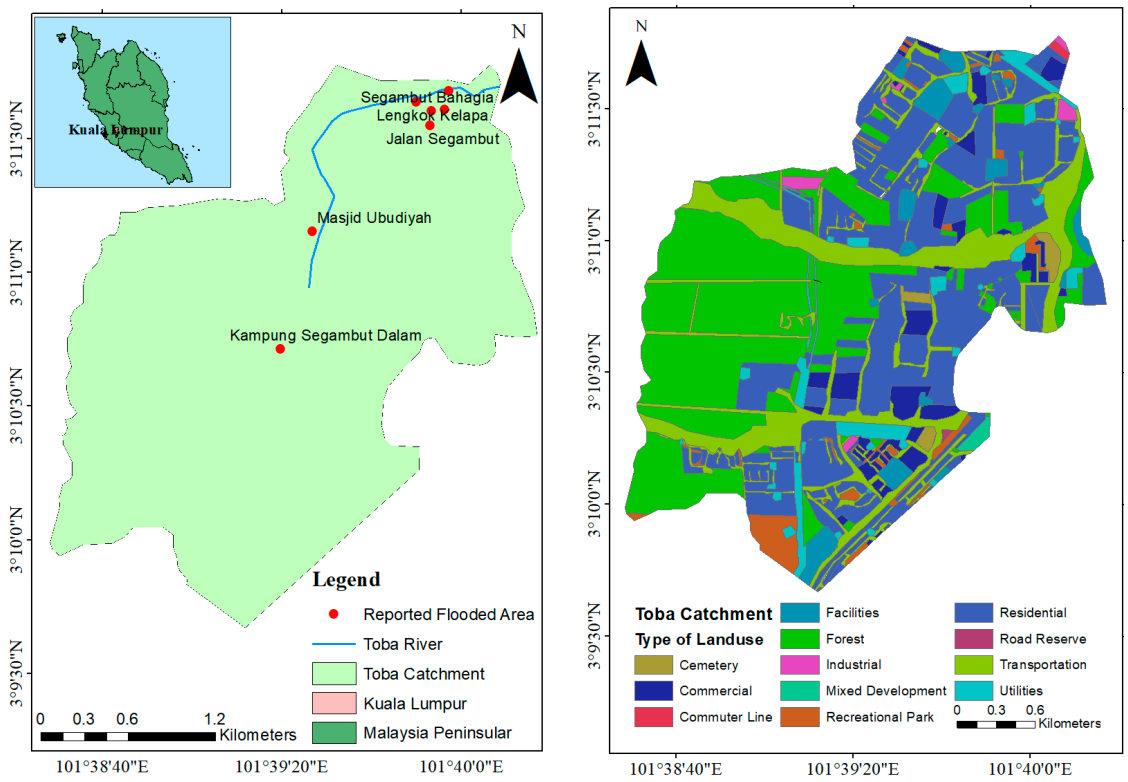

(**a**) (**b**)

Figure 1. The Toba Catchment. (**a**) Reported flood locations with some locations having multiple occurrences, and (**b**) land use map.

Table 1. Reported flood occurrences in Segambut [19].

Reported Locations	Date of Occurrence	Reported Depth (m)	Rainfall Information	
			Storm Duration (h)	Probability of Exceedance [1]
Masjid Ubudiyah	6-Feb-09	0.5	n.a.[2]	n.a.
	14-Oct-19	0.3–0.9	1	88
	14-Feb-20	0.1–0.9	1.5	38
Jalan Segambut	18-Jul-20	0.3	n.a.	n.a.
	18-Apr-12	0.3–0.6	3	n.a.
	16-Sep-16	0.3–1.0	n.a.	n.a.
Jalan Kelapa Muda	18-Apr-12	0.3–0.6	3	n.a.
	21-Aug-12	0.3–0.6	3	n.a.
	16-Sep-16	0.3–1.0	n.a.	n.a.
Segambut Bahagia	3-Apr-18	0.2–0.5	1	0
	18-Apr-12	0.3–0.6	3	n.a.
	21-Aug-12	0.3–0.6	3	n.a.
	12-Sep-12	0.3–0.6	3	n.a.
	6-May-13	0.3–0.7	3	55
	24-Apr-14	0.4–1.0	n.a.	n.a.
	13-Aug-15	1.5	1	29
	4-Sep-15	0.3	n.a.	n.a.
	15-Nov-15	0.3–0.6	1	n.a.
	4-Mar-16	0.3–0.6	1.5	30
	16-Sep-16	0.3–1.0	n.a.	n.a.
Segambut	10-Apr-13	0.3–0.5	2	15
		0.3–0.6	2	20
	3-May-13	0.3–0.7	1	70
Segambut Dalam	10-Oct-13	0.3	3	20
	13-Aug-15	1.5	1	29
	15-Nov-15	0.3–0.6	1	n.a.
Segambut Bahagia Tambahan	16-Sep-16	0.3–1.0	n.a.	n.a.
Segambut Tambahan	26-Apr-17	0.3–1.0	2	13
Lot 1593 Kg. Segambut Dalam	14-Feb-20	0.1–0.9	1.5	38
Lengkok Kelapa	16-Sep-16	0.3–1.0	n.a.	n.a.
Jalan Kolam Air	4-Sep-15	0.3	n.a.	n.a.

Note: [1] IDF curve based on DID. [2] n.a. = not available.

3. Methodology and Data

A flood risk assessment aims to quantify the expected annual damage (EAD) considering the monetary impacts of flooding. Flood risk is determined by flood hazards, exposures and the degrees of vulnerability of those exposed to flooding. This study defines flood hazard as the flood events' probabilities and the corresponding magnitudes of flows [20,21]. Meanwhile, the exposure of elements at risk to floods is determined by flood inundations. Through these definitions, a chain of methodology was developed that consists of three modules (Figure 2). The first module aims to simulate flood inundations from the different DEMs and across a range of different return periods. This is followed by the second module, which quantifies the resulting damages with applications of a vulnerability function alongside the simulated depths and area. Since multiple return periods and an associated DEM are used, the second module involves a repetitive computational process. Lastly, the final module quantifies flood risks using the information of flood probability and damages. The DEM properties are inherent in the first and the second modules, allowing the intermediate and the end results to be linked back to the DEM type and resolution. Furthermore, the methods apply consistent reclassification on spatial data layers from flood inundation to damage calculations to fit the DEM resolution characteristics, which makes the results comparable. Integrating various spatial data layers has been widely undertaken in flood damage and risks assessments (e.g., as reported by Zhou et al. [22]).

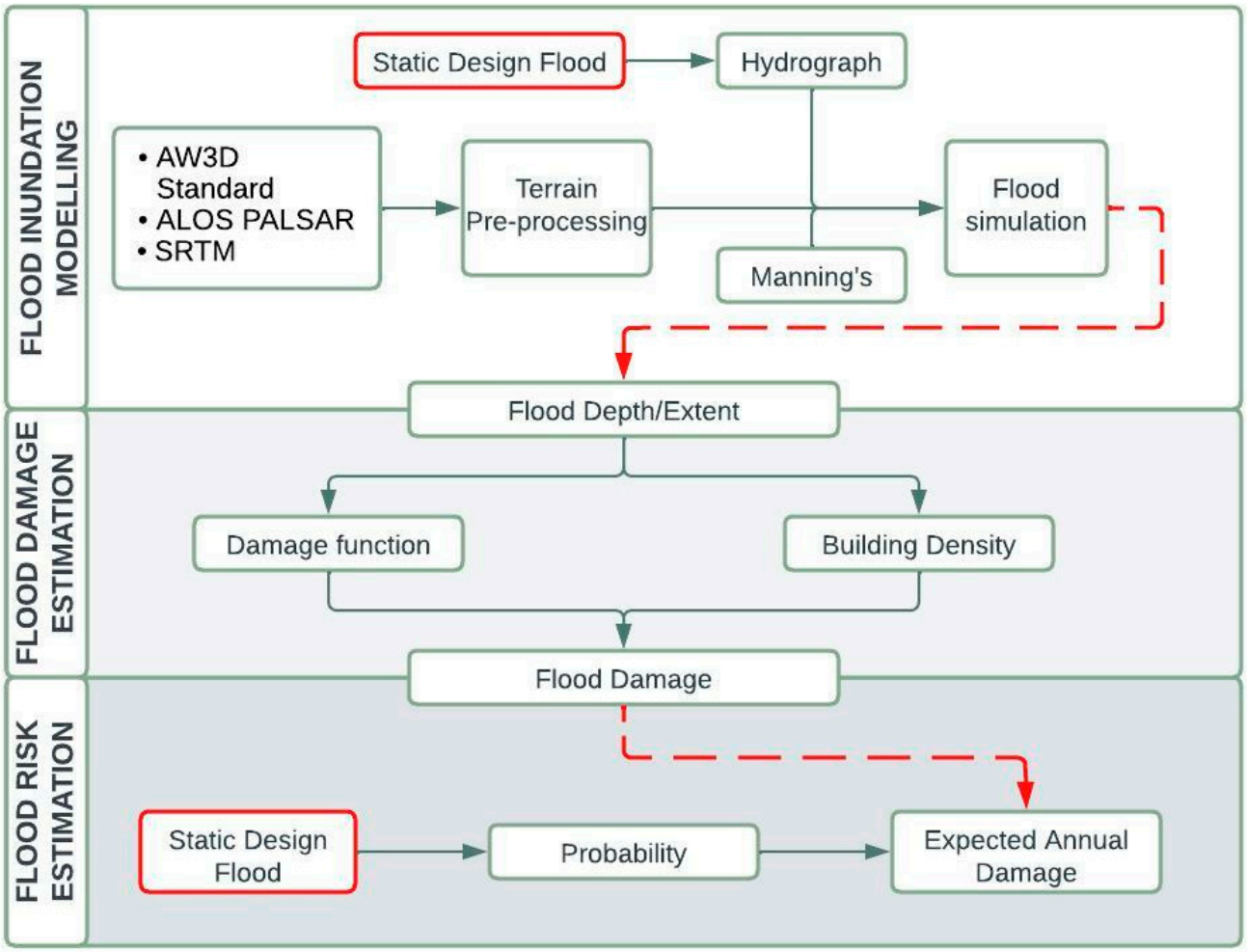

Figure 2. Conceptual workflow for this study. The workflow was repeated for three DEMs with different spatial resolutions.

3.1. DEM Data

Advanced Land Observing Satellite Phased Array L-band Synthetic Aperture Radar, also abbreviated as ALOS PALSAR, is a geometric and radiometric terrain of corrected data product with a pixel size of 12.5 m, generated from high-resolution and medium-resolution DEMs [23]. An optical sensor onboard the Advanced Land Observing Satellite operated from 2006 to 2011 was designed to generate global elevation data [24]. In addition, Advanced World 3D (AW3D) is a product that is generated utilizing the global data archives from five years of observation of the optical sensor [25].

This study compared the application of DEM from the Shuttle Radar Topography Mission (SRTM) at 30 m resolution, ALOS Phased Array type L-band Synthetic Aperture Radar Mission (ALOS PALSAR) at 12.5 m resolution [26] and the 5 m resolution of AW3D Standard. The first two datasets are available for most areas on Earth and are freely accessible to the public (Appendix A). The third is a finer resolution commercial DEM product obtained from the provider. Unlike the 30 m resolution AW3D (AW3D30), which is freely accessible to the public, the 5-m resolution AW3D Standard is not yet freely available. The SRTM data for the study area were downloaded from the official website of the U.S. Geological Survey [27]. ALOS PALSAR was obtained from Alaska Satellite Facility (ASF) Distributed Active Archive Centre (DAAC). The variation in DEM used in the study was used to compare the effects of DEM resolution in damage and risk estimation of floods.

In most cases, DEM provides poor riverbed profiles because of the failure of remote sensors to penetrate water surfaces [11,28]. The loss of river profile is a common issue

for small rivers but less so for larger rivers [29,30]. This is evident in [31], where they discovered that the absence of river channel characteristics is not very apparent until the DEM resolution goes above 10 m, though this also depends on the river width. In order to reduce the error, studies have suggested using a finer-resolution DEM for the channel and a lower resolution DEM for the floodplain [31]. This eliminates the need for survey information on the in-channel; there is evidence that it can produce acceptable flood inundation simulations [31]. Understandably, flood simulations would be better if survey information of in-channel bed elevation is included, as suggested in [29,30,32]. However, this relies on data availability and other constraints, such as computational expenses.

During the preparation of inundation simulations, it was found that the Toba River was not detected in GIS. This was likely due to the size of the river width being smaller than the size of the DEM cell. Terrain modification for all three DEMs was therefore undertaken. The riverbed elevations and widths from multiple surveyed cross-sections of the actual river obtained from the authority were generated in the DEM to establish the flow path for inundation simulations. The in-river geometry was then interpolated and resampled into smaller size pixels of 0.25 m before being merged with the floodplain terrain data of the original DEM. The final products after modification (Figure 3), within which the river channel has been resolved, were used in the hydrodynamic simulation.

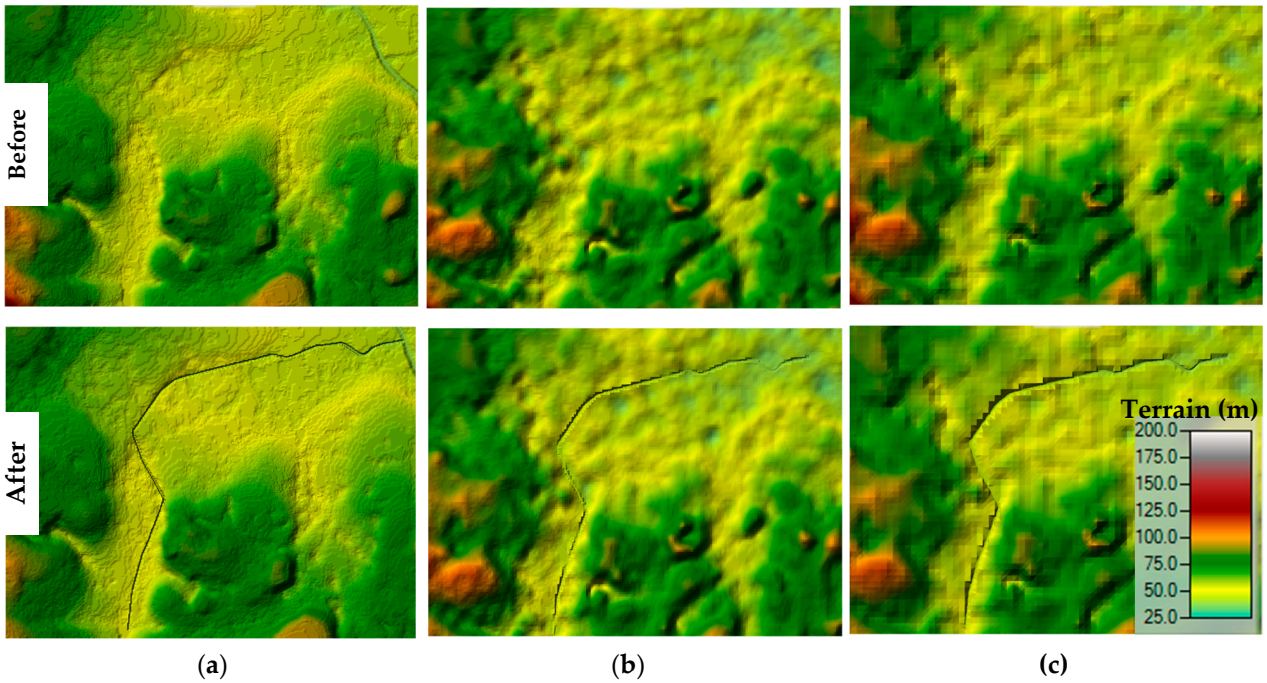

Figure 3. Maps of before and after modification of DEM terrain in Toba Catchment: (**a**) AW3D Standard, (**b**) ALOS PALSAR and (**c**) SRTM.

3.2. Flow Data

In any quantitative flood risk study, information on flow-probability relations is essential. The Toba River catchment is an ungauged catchment, and historical flow records are not available. This study constructed a flow–probability relationship based on information in the 2015 Toba River flood alleviation scheme report [33]. In the 2015 flood study, the Toba River catchment is divided into 43 subcatchments with a range of areas between 0.1 and 0.5 km^2 for rainfall–runoff simulations. HEC–HMS model was then applied for storm durations of 0.5, 1, 2 and 3 h to arrive at a critical storm duration of 1 h. The peak flows corresponding to the critical storm duration were simulated in the 2015 study for 2, 5, 10, 20, 50 and 100-year return periods. Based on a 1D-hydrodynamic simulation from MIKE 11 at the 100-year return period peak flow, the 2015 study successfully reproduced

the exceeding water levels in some sections along the river. This reflects the realistic values of the peak flows simulated from the 2015 study.

Following the reported peak flows—probability information from the 2015 report, the present study extended the relationship to account for probable magnitude of a 1000-year return period event using a power model fit (Figure 4). Furthermore, 3- and 4-year return period events were also added to arrive at a total of six design flood events. The returned peak flows are in the range of 7.45 to 22.91 m^3/s. The overall small magnitude of discharge implies the relatively small catchment and the location of the catchment at the upstream location of Klang River Basin.

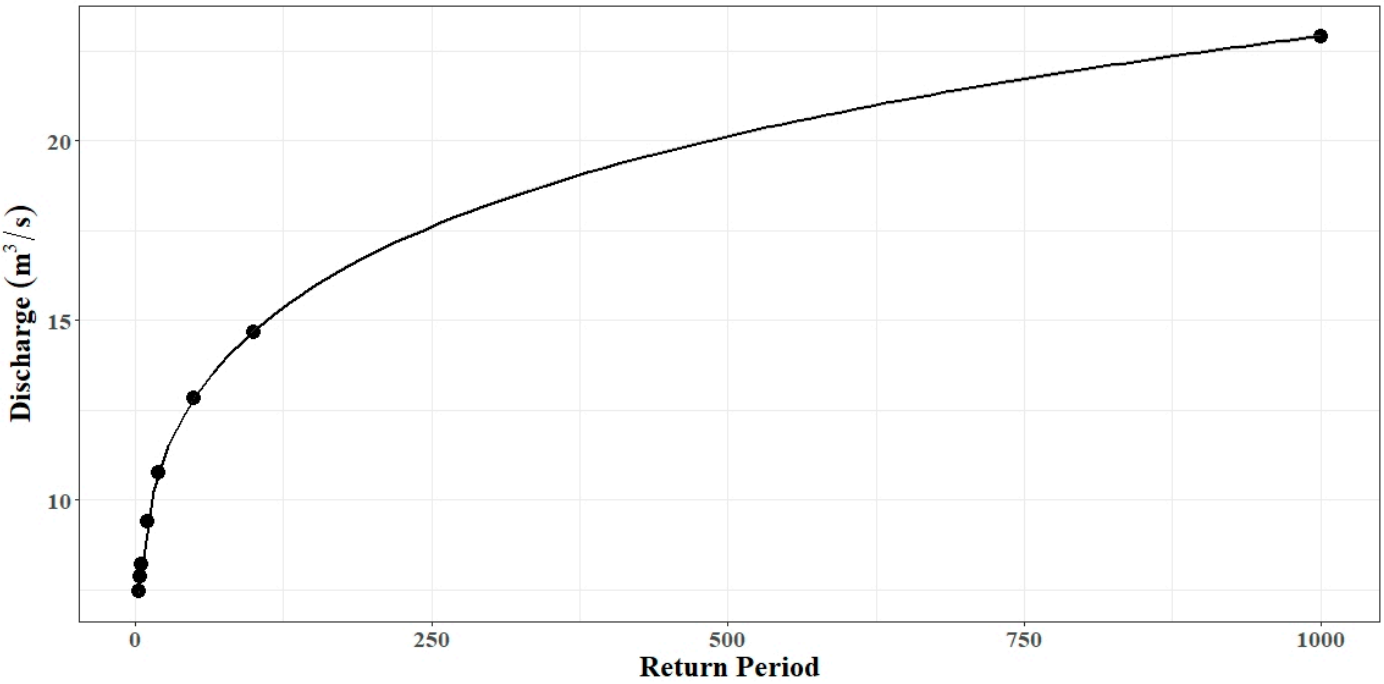

Figure 4. Peak flow–return period relationship of the Toba River.

3.3. Land Use, Cross-Sections and Manning's Data

For use in the hydrodynamic modelling, riverbed level and width from 22 surveyed lateral cross-sections of the Toba River from the DBKL report [33] were integrated into the DEM, and a from land-use map of 2020 obtained from the authority in printed copy was digitized, as presented in Figure 1b. Based on the land use map, there is about 32% forested area, and the rest of the area is dominated by residential land. It was reported in the 2015 flood study that the river surface is mostly made up of concrete at the upstream site, and gabion and rubble pitching at the downstream section. In HEC-RAS, Manning's value was set as 0.015 for the longitudinal section lined with concrete, and 0.030 and 0.035 for the gabion and stone pitching, respectively [34]. Manning's n for residential, commercial, utilities, facilities, transportation, industrial, mixed development and commuter lines was set as 0.15; it was 0.025 for barren land, which is generally covered by 15% road reserves and cemeteries. Meanwhile, a recreational park and a mixture of land areas (e.g., some constructed materials, but mostly vegetation in the form of lawn grasses) were set to have Manning's n of 0.04. For the forest land area, the manning roughness was set as 0.16. These values were specified as suggested in Curtis [35], which adopted the values from various studies (i.e., [34,36]).

3.4. Flood Inundation Modelling

The HEC-RAS model was developed by the Hydrologic Engineering Centre of the Institute for Water Resource for the United States Army Corps of Engineers and has been

widely used in hydrology and hydraulic modelling. Examples of applications of the 1D HEC-RAS model can be found in [37,38], and in the 2D hydraulic model by Bates and De Roo [39], among others. It is widely acknowledged that inundation extents predicted by a 2D model are more realistic and accurate compared to a 1D approach because of the small variability in its predictions for different topographic and geometric representations [28].

In this study, flood inundation was simulated using HEC-RAS 2D hydraulic modelling by assuming the flow was unsteady through the diffusion wave equations, which characterise the movement of water under the forces of gravity and friction. The model is facilitated by the river and floodplain discretization into 2D mesh cells [40] and adopts a sub-grid bathymetry technique [41] that uses both the hydraulic and geometric property tables that represents the cell and cell faces from the sub-grid terrain.

With the assumption of incompressible flow, the unsteady differential form of the mass conservation (continuity) equation is:

$$\frac{\partial H}{\partial t} + \frac{\partial (hu)}{\partial x} + \frac{\partial (hv)}{\partial y} + q = 0 \quad (1)$$

where t is time; u and v are the velocity in x- and y-direction, respectively. H is the water surface elevation and defined as the sum of surface elevation z (x, y) and water depth h (x, y, t); q is the source/sink flux term.

A key parameter in hydraulic modelling is the resolution of the mesh, which controls the movement of water through the 2D flow area [36]. A smaller mesh size typically leads to greater accuracy, but also results in a longer computation time and a larger virtual memory requirement. We fixed the mesh size at 5 m across all simulations. The model configuration also includes the step of specifying the internal upstream condition within the 2D boundary, and the external downstream boundary is located outside the 2D flow area at normal depth as an indication that the water flows out of the 2D flow area. The input hydrographs are governed by the peak flows generated from the hydrological modelling, as presented in Section 3.2.

The simulations were applied to AW3D Standard, ALOS PALSAR and SRTM DEMs using the same hydraulic configurations. The model generated unique flood inundation maps for the different flood events and DEM data. Simulated flood characteristics were then analysed using the HEC-RAS built-in tools (i.e., RAS Mapper) and external GIS tools.

3.5. Flood Damage Estimation

This study focuses on flood damage to residential buildings. A depth–damage function of a single residential building was used as a sub-function of the total damage estimation. The depth–damage function represents the susceptibility of buildings to direct physical damage when in contact with floodwater. The function has been widely used in flood risk assessment (e.g., [42–47]). The function is explained in Section 3.5.1, followed by the total damage function in Section 3.5.2.

3.5.1. Depth–Damage Relationship

A depth-damage function is commonly developed from a dataset formed through systematic surveys and/or questionnaires, with or without insurance claims and data, and may involve synthetic data development [33,38]. The depth–damage curve used in this study was the official flood damage function for Malaysia established in [48,49]. It was derived from multiple regressions over questionnaire data, hence providing a set of fixed coefficients values in the function. Equation (2) shows the explanatory variables of the damage factors used in the function: flood depth in meters, z; flood duration in days, t; and residential area strata state, F. Strata state, s, uses a binary classification; 1 refers to an urban area and 0 refers to a rural area. The mean values associated with the variables are provided as constants in the function (i.e., 0.93, 2.83 and 0.25). The damage factor needs to

be multiplied by the mean building damage, given as RM 3273.58, to obtain the monetary direct damage, d_z, where subscript z is the flood depth increment.

$$F = (z - 0.93) \times 0.32 + (t - 2.83) \times 0.08 + (s - 0.25) \times 0.33 + 1 \quad (2)$$

$$d_z = F \times 3273.58 \quad (3)$$

A 6 h flood duration was used based on reports of previous flood events in the Toba River, and the residential area classification, s, was chosen as 0 for a non-urbanized area. The duration and residential area classification in the equation were fixed to constant values, and flood depth varied depending on the inundation depths.

3.5.2. Direct Damage of Flood

In this study, the threshold of damage was set to be when flood depth surpasses the building's ground level. It was assumed that the building's ground levels are provided by the DEM layer. The total damage over the entire flooded area of a given flood event was estimated by integrating the damage at flooded pixels. All the flooded cells were classified by flood depth increments for analytical computation of the total damage;

$$D_T = \sum_{z=1}^{Z} A_z H_A d_z \quad (4)$$

where D_T is the total damage for a flood event, T; A_z is the number of cells; and H_A is the number of residential buildings in each cell.

Information from the land-use map, DEM and flooded area for each flood return period was overlaid with GIS tools to identify flooded cells. These were then classified according to flood depth. The size of each cell for damage calculation was specified as 625 m^2 and consisted of four buildings based on typical residential building density in Malaysia, which was deduced from satellite imagery [50]. To maintain the initial resolution of ALOS PALSAR and SRTM for the damage assessment, we fixed the pixel size to 900 m^2 (30 m × 30 m) for SRTM, 156.25 m^2 (12.5 m × 12.5 m) for ALOS PALSAR and 25 m^2 (5 m × 5 m) for AW3D Standard. For SRTM and AW3D Standard, the number of buildings was mathematically suited to the cell size ratio to perform the damage calculation. To classify the cells, we chose 0.3 m depth increments up to the highest inundation depth. The small incremental interval chosen was aligned with the micro-scale assessment in which the heterogeneous impact on buildings in the flooded area is emphasized (e.g., [44]). This helped to distinguish the effects of the DEM resolution on flood damage and risk. By computing D_T for all considered flood events, the relation of total damage and flood probability was obtained and used to form a probability–damage relation for subsequent risk estimation.

3.6. Flood Risk Estimation

The established probability–damage relation provides essential information for quantifying flood risks. The average damage at each interval of flood probability, together with the difference in probability at the interval, were integrated to determine the expected annual damage.

$$\text{Risk} = \sum_{T=1}^{N} (p_{T+1} - p_T) \cdot \frac{(D_{T+1} + D_T)}{2} \quad (5)$$

where p is the probability of a flood event, T, and D is the damage of the flood event. The equation has been widely used and applied as an approximation to compute the area under the probability–damage curve [42,45,47].

4. Results and Discussion

4.1. Flood Inundations

Flooded areas and median depths extracted from flood inundation maps of different return periods are presented in Table 2 (the first three main columns). The simulated flooded area increases with the return period. Similar percentage increases for 3- and 100-year return periods can be observed for all three DEMs. The inundation areas with AW3D Standard increased by 22%, 12% and 9% between 3 and 20-year return periods, 20- and 50-year return periods and 50 and 100-year return periods, respectively. For the same periods of comparison, inundation areas with ALOS PALSAR increased 23%, 13% and 12%, respectively; with SRTM, the values increased by 24%, 10% and 9%, respectively. There was a moderate decrease in the percentage difference of flooded areas over the higher return period, which is similar to the findings reported by Banjara [51], where the author found that simulated flooded areas increase dramatically between 5- and 25-year return periods, but only moderately increase over higher return period floods. This reflects the relationship between flows and probability, where changes in flow with a high probability of flooding are deemed to be smaller. Therefore, the resulting marginal changes in flooded areas are not as widespread as in between the more frequent floods (Figure 4). However, this cannot be generalised, as the flow dynamics also depend on the characteristics of the land surface.

Table 2. Results of total inundation area, median flood depth, total damage and flood risk in expected annual damage.

Return Period (Year)	Inundation Area (km^2)			Median Floodplain Depth (m)			Total Damage (RM in Million)			Expected Annual Damage (RM in Million)		
	A3	AP	SR	A3	AP	SR	A3	AP	SR	A3	AP	SR
3	0.20	0.09	0.06	0.62	1.36	0.80	2.95	1.88	0.96	1.15	0.70	0.37
4	0.21	0.09	0.06	0.67	1.37	0.80	3.11	1.93	0.99			
5	0.21	0.10	0.06	0.68	1.35	0.83	3.2	1.96	1.00			
10	0.23	0.10	0.06	0.78	1.34	0.89	3.54	2.11	1.08			
20	0.24	0.11	0.07	0.81	1.25	0.84	3.68	2.30	1.25			
50	0.27	0.13	0.08	0.93	1.25	0.92	4.52	2.62	1.41			
100	0.30	0.14	0.09	0.98	1.21	0.94	5.03	2.93	1.54			
1000	0.35	0.18	0.14	1.01	1.52	1.13	6.58	3.95	2.55			

Note: A3 = 5 m A3WD Standard, AP = 12.5 m ALOS PALSAR and SR = 30 m SRTM.

Comparisons between inundation area generated on the floodplain from the three DEMs show that a higher resolution DEM results in a larger flooded area as compared to a coarser-resolution DEM, regardless of the return periods (Table 2). On the other hand, comparisons between the median flood depths show an inconsistent trend, where the highest median flood depth is from ALOS PALSAR DEM and not from the highest resolution DEM, i.e., AW3D Standard. Meanwhile, a general increment of median flood depth can be observed for AW3D Standard over higher return period, but is not apparent for ALOS PALSAR and SRTM. The median flood depth considers depths at the individual flood cells over the entire flooded area, and hence is subjected to not only the flooded area but indirectly to the number of flooded cells. Given that each DEM is subjected to different resolutions (and elevation information within each cell), comparisons using only the expected flood depth can be deceiving. Further visualisation of the relation between the variation of flood depths and the percentage of inundation cells over the entire flooded area with respect to the DEM and return period (Figure 5) revealed that it is not possible to establish a correlation between simulated flood depths and DEM type and resolution. Nevertheless, the distribution of flood depth percentage area was found to be skewed for all three DEMs. This highlights the dominating shallow flood depths from the range of return period events across the three DEMs.

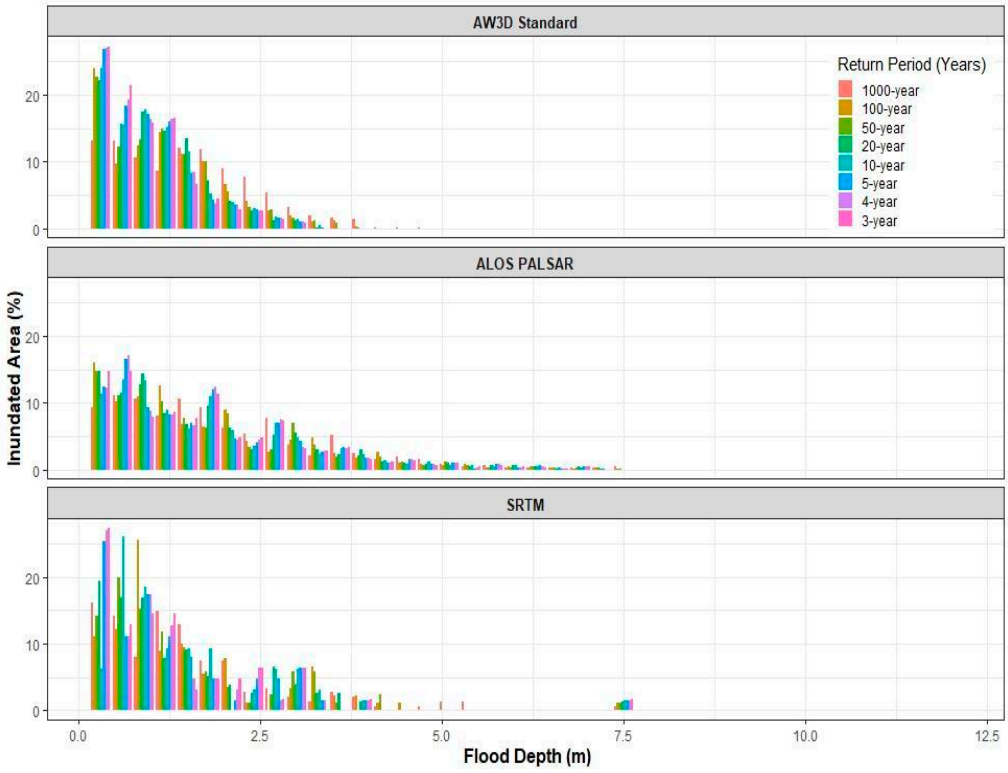

Figure 5. Distribution of flood depths across the floodplain areas of AW3D Standard, ALOS PALSAR and SRTM. Results from all flood events are shown. The *y*-axis is the percentage of inundation area over the total inundation area for each considered flood depth.

Figure 6 shows a 100-year return period inundation map between the three DEMs. There were multiple overlaps in both upstream and downstream areas between the simulated and the reported flood area; areas were generally larger on the downstream ends. Simulated inundation area using AW3D Standard overlayed the most area reported flooded compared to the other two DEMs. This indicates that the ability of AW3D Standard to predict flood extent is greater than the other two DEMs. Nevertheless, the coarser DEM resolution also shows good agreement at some locations. Ideally, the accuracy of the simulated flood depths against the reference case (e.g., from a benchmark model such as LiDAR) is measured using indicators, such as the fit index [52]. Such comparisons are not viable in this study, owing to the absence of a very fine resolution DEM.

It is apparent that the inundation area, especially at the low-laying region downstream of Toba River of the coarser-resolution DEM, is much smaller as compared to the finer-resolution DEM (as provided in Table 2). This is paralleled by the findings from other studies showing that coarser DEM resolution results in smaller flooded area. For example, Cook and Merwade [28], when investigating the effects of topographic data, geometric configuration and modelling approach on flood inundation mapping using LiDAR, 10 m and 30 m DEM, found that the area of flood inundation decreases with higher spatial resolution. Zhang [53] also found that the inundation extents using a coarser-resolution SRTM-DEM are smaller than with the LiDAR-DEM. The larger inundation area from a coarser DEM type is likely to be influenced by the considerable anomalous of its ground elevation being smoothed into coarse values by the surrounding lower latitudes, resulting in greater flood depths on certain cells [54]. The greater flood depths on cells of the coarse DEM due to the smoothing effect can be seen in Figure 5. A number of cells with unusual higher values of flood depths are shown that are from SRTM DEM, but not from A3WD and ALOS PALSAR. Furthermore, the smoothing effects may result in extreme inundation areas being ignored if relatively local low-laying regions exist. As a result, the inundation area from the simulation is expected to reduce. The sample cross-sections of SRTM and ALOS

PALSAR in Figure 6 (D) upstream, (E) midstream and (F) downstream exemplify how local low-laying regions may have caused reductions in simulated flooded area when compared to the A3WD. A smaller slope variability from finer-resolution DEM also resulted in a greater flooded area from A3WD as compared to the other two DEMs. As discovered by Garrote [55], coarser DEM has higher slope variability than finer-resolution DEM, which may cause the flow to spread more freely on the floodplain, hence inundating more areas. The higher slope variability is due to its coarser resolution, which causes random land cells' elevation levels to be much higher compared to the finer-resolution DEM [31].

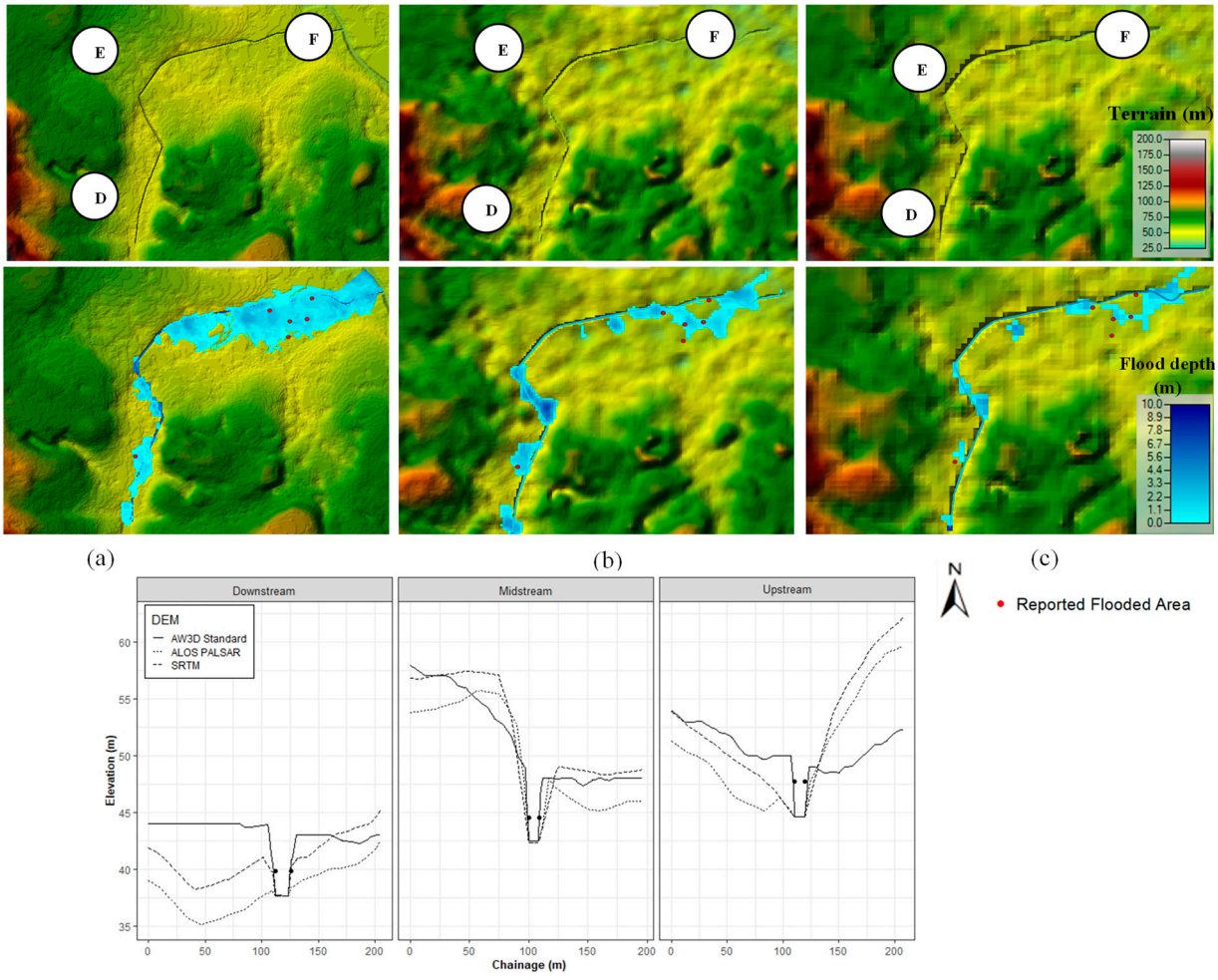

Figure 6. River cross-sections at three different locations: D = upstream, E = midstream and F = downstream. Black dots in the cross-sections are referring to the riverbank. Flood maps of simulated flooded area and depths from 100-year return period event for (**a**) AW3D Standard (**b**) ALOS PALSAR and (**c**) SRTM. Reported flooded locations are in red dots.

Channel characterizations are another factor that inevitably affects simulated depth and area [56,57]. The present study superimposed lateral riverbed levels and widths on the Toba River channel cross-sections but ignored the cross-sections' full dimensions. The interpolations that merged the bed level and the original DEM caused the final river geometry to vary across the DEMs. As a result, the river capacity and propagation of flood water differ between DEMs. Unless actual measurements of extremely detailed and accurate river geometry are used in the model, the river capacity is only a rough representation of that of the real river channel. Nevertheless, the merged AW3D Standard exhibits a better proportion of river cross-sections as compared to the other two, especially in the downstream section (Figure 6). This indicates that the representation of the merged A3WD DEM better reflects the existing channelised river of the study area, which adds

confidence that the modified-river and A3WD floodplain DEM is better in representing the channel than the other two DEMs, conforming the findings of the overlayed inundation map with reported flood locations.

Some studies have highlighted that the aptness of the size of DEM resolution depends on the severity of events and modelling purposes. Sanders [58] explained that the flood frequency can influence the suitability of DEM and added that a finer-resolution DEM is preferred for relatively frequent floods (i.e., 2–10-year events). This is because a finer-resolution DEM is better for reproducing small channels that are likely associated with frequent floods. However, the finer-resolution DEM is less important for modelling severe and less frequent floods (e.g., dam break events). A coarse-resolution DEM may not be suitable for detailed designing of hydraulic structures, yet it is beneficial to support flood mapping as a non-structural measure to raise awareness and educate people living in flood-prone area [59]. Hence, coarse DEM can be applied to support structural and non-structural measures.

4.2. Estimation of Flood Damage and Risk

The total economic damage in Ringgit Malaysia (RM) was calculated using Equations (2)–(4). Alongside the return period (or probability), flood damage–return period curves were produced for AW3D Standard, ALOS PALSAR and SRTM. The curves appear to exhibit similar incremental patterns over the higher return periods (Figure 7). The concave shape of the damage–return period curves (or the convex shape of the damage–probability of exceedance curves) from all DEMs depict the expected reduction of the damage rate over the higher return period, which conforms with the rate of inundation area (Table 2). The damage increment was 100% from the lowest to the highest return period considered across all DEMs. The total damage for any specific event at the Toba River is expected to be greater than RM 1 million. In terms of flood risk, the expected annual damage reaches up to RM 1.2 million.

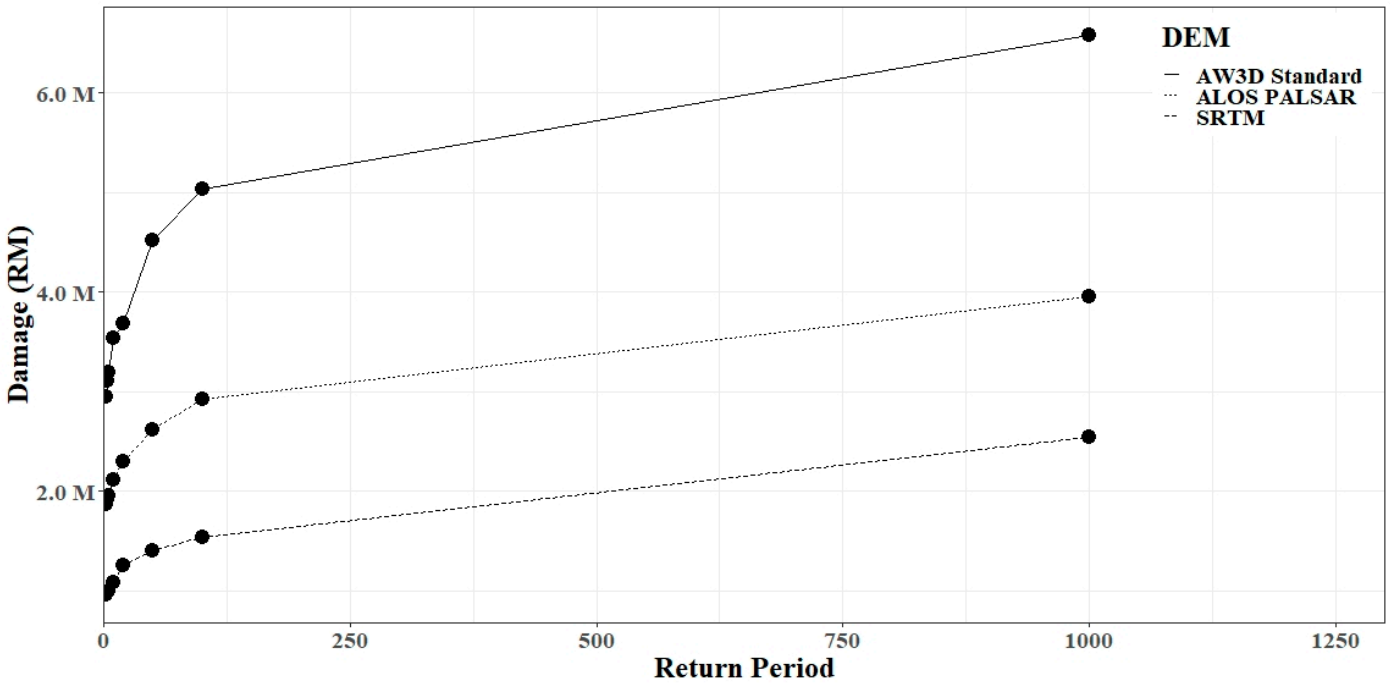

Figure 7. Flood damage estimates for AW3D Standard, ALOS PALSAR and SRTM with interpolation lines. Bullet dots refer to the total damage for each flood event.

Previous studies have shown that damage estimation is difficult to validate because of limited and incomplete historical damage data [45,48,60,61]. The present study also

faced the same challenge because of a lack of historical data and unavailability of insurance claim information; hence, validation of the EAD estimates was not possible. The calculated damage is also prone to a certain degree of uncertainty due to adaptation performed by some residents. Frequent occurrence of flooding results in people adapting to flooding by modifying their houses. The construction of a concrete blocks of low walls and raising the plinth levels of their houses were some of the structural measures implemented by residents [62].

The flood damage and risk results highlighted the importance of considering discrete flood depths over the flooded area. For example, although flooded areas of 3- and 4-year return period events for SRTM are similar and the median flood depths of the two are the same (Table 2), the difference in their aggregated damage is RM 0.02 million. Furthermore, the inclusion of low and high probability flood events leads to an improved flood risk estimate. Floods with relatively small return periods (or high exceedance probability) exhibit low economic damage per event. Still, due to being a frequent occurrence, it should be considered in the whole assessment of risk, as the potential impact may extend far greater than expected [63].

Three resolutions of DEM were applied here, and the analysis showed that estimates of flood damage and risk were at their greatest for the 5 m AW3D Standard, followed by 12.5 m ALOS PALSAR and 30 m SRTM. This highlights that the finer-resolution DEM resulted in greater flood damage estimates and EAD than when a coarser DEM was used. Furthermore, the influences of DEM resolution on flood damage and risk estimates are aligned with the increase in flooded areas (Section 4.2), but not with the distribution of flood depth or median flood depth (Figure 8), as the trend of median flood depth shows inconsistency across the resolution of DEM. This observation emphasizes the importance of integrating the area and depth for the effects of DEM resolution to be better understood in a risk-based assessment of flooding instead of a fragmented approach that considers only one of the flood parameters (e.g., flood depth).

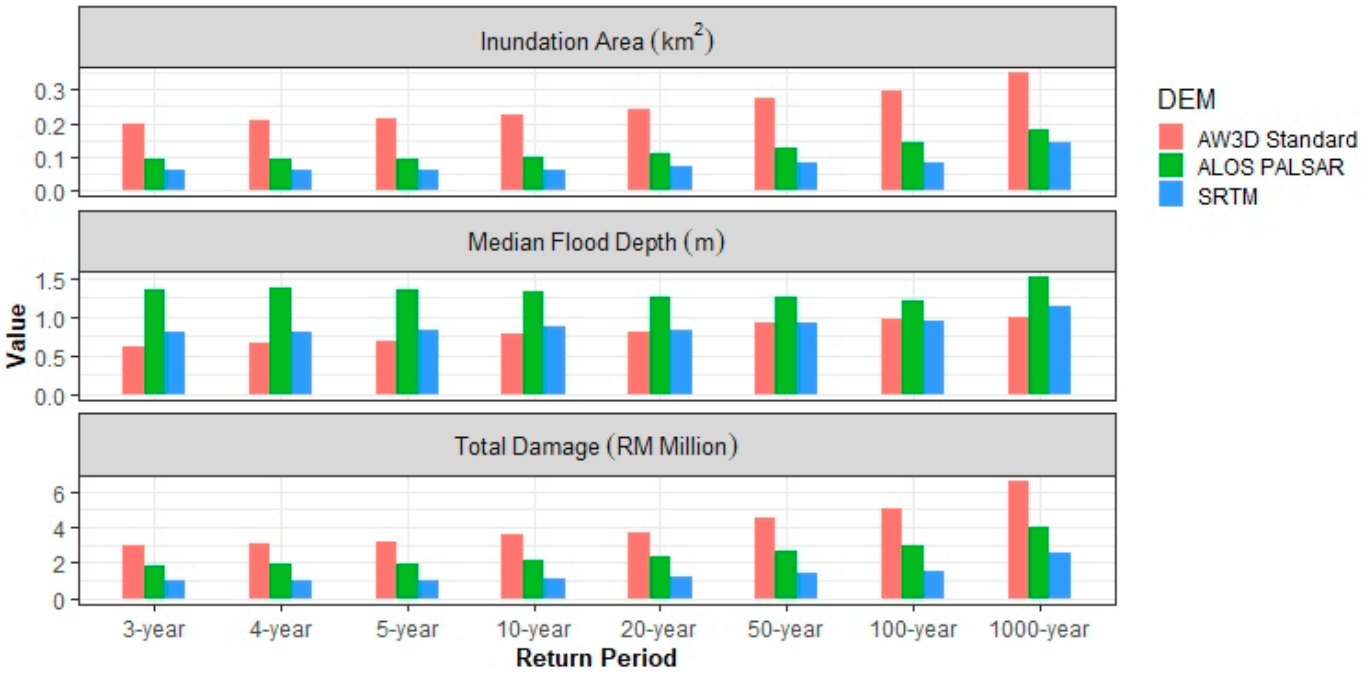

Figure 8. The output comparisons of AW3D Standard, ALOS PALSAR and SRTM.

4.3. Limitations and Recommendations for Future Works

Several limitations were inherent in this research given that it was based on a small sub-catchment area. First is the absence of a gauging station in study area. Flow and water level data are the key data for simulating flood inundation, as it is essential for the model

to compute the volume of water that the channel can contain before overflowing into the floodplain and inundating the nearby area. Then, the DEM spatial resolutions applied in this study were coarse. Finer-resolution measurements, such as LiDAR, will provide better accuracy; however, LiDAR is not cost-effective, and data collection is time-consuming. Hence, for future works, it is recommended to improve the DEM datasets for this proposed methodology. Finer resolution offers better accuracy when representing the topographic features. Flood risk assessment at the micro-scale level would be upgraded and could help increase the reliability of risk-based flood decision making at the local level.

The non-availability of local damage data or a flood map for the study area was a drawback to the validation process. The application of the national damage function in a local study may result in the overestimation of damage and risk computation. The damage and risk estimation for the present study focused on the impact due to flood depth only. Therefore, the damage and risk estimation could be expressed in other functions that depict the influences of other flood factors than flood depth. Other relevant hazard indicators for a flood (i.e., flood duration, velocity and time of occurrence) could also play big roles in the damage function. Not only that, but the proposed methodology could be extended with another type of land use (commercial, transportation, etc.). As mentioned previously, this study was conducted for one particular research area; hence, a similar study of another area with distinctive topography, hydrological characteristics and size would be worth exploring. However, the detail setting of the methodology could be altered accordingly to fulfilling the needs and limits of the study. For example, consider the application of a reasonable mesh size to maintain the numerical accuracy (i.e., computational needs).

5. Conclusions

The use of DEM greatly assists flood damage and risk assessment, yet the type of DEM used is inevitably constrained by the availability and financial resources. Furthermore, poor representations of rivers may require a pre-treatment of DEM before the assessment could be made. Very few studies have explored the effects of super-imposed river terrains paired with the DEM's original form for floodplain on flood damage and risk estimates. Moreover, the effects of different DEM resolutions in this regard have not yet been explored. This study aimed at investigating the relative benefits of applying different DEMs with riverbed modifications to damage and risk estimates. A methodology was proposed to carry forward the spatial characteristics into 2D inundation modelling, followed by the damage and risk estimations. The simulated depths and areas from the three DEM sources used, AW3D Standard (5 m resolution), ALOS PALSAR (12.5 m resolution) and SRTM DEM (30 m resolution), governed the final risk estimates.

The findings from this study show that the application of finest resolution DEM (AW3D Standard) with modified riverbed terrain yielded the best performance in the simulating flooded area. Nevertheless, the coarser resolution of DEM (SRTM) with improved riverbed terrain also agreed with many reported flooded areas. Implementation of building-level damage analysis further showed that the use of the DEM with finer resolution almost doubles the estimated flood damage severity and the flood risk compared with the use of a much coarser-resolution DEM. This finding highlights the potential advantage of using a finer-resolution DEM for flood risk management. Overall, the simulation outputs exhibit notable relationships between DEM resolution, inundation area, and flood damage and risk, but not for median flood depth. This emphasises caution when comparisons are being performed on the basis of expected flood depth over a large inundation area.

The application of global DEMs has aided risk-based decisions about the use of hard measures (mainly structural, such as engineering interventions) or soft measures (mainly non-structural, such as policy development) at the local, catchment or national levels [9,58]. For large-scale assessments, the use of a global DEM compensates for the absence of local-resolution DEM and reduces the time and cost of data acquisition [9,64]. The methodology developed here could prove beneficial for such assessments and can be readily expanded to include other sectors that are at risk, such as commercial sectors or infrastructure facilities.

Author Contributions: Conceptualization, E.F., B.M.R., P.R., V.A.B., Z.Z. and B.Y.; data curation, B.M.R.; formal analysis, E.F.; funding acquisition, B.M.R.; investigation, E.F.; methodology, E.F. and B.M.R.; project administration, B.M.R. and V.A.B.; resources, E.F. and P.S.; software, E.F.; supervision, B.M.R., P.R. and V.A.B.; validation, P.R. and B.M.R.; visualization, E.F.; writing—original draft, E.F.; writing—review and editing, E.F., B.M.R., P.R., V.A.B., Z.Z., B.Y. and P.S. All authors have read and agreed to the published version of the manuscript.

Funding: This work is part of the project 'Flood Impact Across Scales', funded under the Newton-Ungku Omar Fund 'Understanding of the Impacts of Hydrometeorological Hazards in South East Asia'. The grant was jointly awarded by the MYPAIR Scheme under the Ministry of Higher Education of Malaysia (NEWTON/1/2018/WAB05/UPM/2) and the Natural Environment Research Council (NE/S003177/2).

Institutional Review Board Statement: Not applicable.

Informed Consent Statement: Not applicable.

Data Availability Statement: Not applicable.

Acknowledgments: The authors are thankful for data sharing and assistance from the Department of Irrigation and Drainage Malaysia, and the Kuala Lumpur City Hall. The authors would like to thank Sayers and Partners LLP for making the DEM data (AW3D Standard DEM) available for this work.

Conflicts of Interest: The authors declare no conflict of interest.

Appendix A

The freely available DEM for this study can be downloaded from the following web pages:

1. ALOS PALSAR DEM: https://search.asf.alaska.edu/# (accessed on 22 June 2020).
2. SRTM DEM: https://earthexplorer.usgs.gov/ (accessed on 22 June 2020).

References

1. United Nations Office for Disaster Risk Reduction (UNISDR); Centre for Research on the Epidemiology (CRED). *Economic Losses, Poverty and Disasters 1998–2017*; United Nations Office for Disaster Risk Reduction: Geneva, Switzerland, 2017.
2. Jongman, B.; Ward, P.J.; Aerts, J.C.J.H. Global Exposure to River and Coastal Flooding: Long Term Trends and Changes. *Glob. Environ. Chang.* **2012**, *22*, 823–835. [CrossRef]
3. Jha, A.K.; Bloch, R.; Lamond, J. *Cities and Flooding: A Guide to Integrated Urban Flood Risk Management for the 21st Century*; The World Bank: Washington, DC, USA, 2012.
4. Salman, A.M.; Li, Y. Flood Risk Assessment, Future Trend Modeling, and Risk Communication: A Review of Ongoing Research. *Nat. Hazards Rev.* **2018**, *19*, 04018011. [CrossRef]
5. Quesada-Román, A. Flood Risk Index Development at the Municipal Level in Costa Rica: A Methodological Framework. *Environ. Sci. Policy* **2022**, *133*, 98–106. [CrossRef]
6. Aroca-Jiménez, E.; Bodoque, J.M.; García, J.A. How to Construct and Validate an Integrated Socio-Economic Vulnerability Index: Implementation at Regional Scale in Urban Areas Prone to Flash Flooding. *Sci. Total Environ.* **2020**, *746*, 140905. [CrossRef] [PubMed]
7. Prakash Mohanty, M.; Nithya, S.; Nair, A.S.; Indu, J.; Ghosh, S.; Mohan Bhatt, C.; Srinivasa Rao, G.; Karmakar, S. Sensitivity of Various Topographic Data in Flood Management: Implications on Inundation Mapping over Large Data-Scarce Regions. *J. Hydrol.* **2020**, *590*, 125523. [CrossRef]
8. Granados-Bolaños, S.; Quesada-Román, A.; Alvarado, G.E. Low-Cost UAV Applications in Dynamic Tropical Volcanic Landforms. *J. Volcanol. Geotherm. Res.* **2021**, *410*, 107143. [CrossRef]
9. Yan, K.; Tarpanelli, A.; Balint, G.; Moramarco, T.; Baldassarre, G. Di Exploring the Potential of SRTM Topography and Radar Altimetry to Support Flood Propagation Modeling: Danube Case Study. *J. Hydrol. Eng.* **2015**, *20*, 04014048. [CrossRef]
10. McClean, F.; Dawson, R.; Kilsby, C. Implications of Using Global Digital Elevation Models for Flood Risk Analysis in Cities. *Water Resour. Res.* **2020**, *56*. [CrossRef]
11. Bhuyian, M.N.M.; Kalyanapu, A. Accounting Digital Elevation Uncertainty for Flood Consequence Assessment. *J. Flood Risk Manag.* **2018**, *11*, S1051–S1062. [CrossRef]
12. Merz, B.; Kreibich, H.; Schwarze, R.; Thieken, A. Review Article "Assessment of Economic Flood Damage." *Nat. Hazards Earth Syst. Sci.* **2010**, *10*, 1697–1724. [CrossRef]
13. Thieken, A.H.; Apel, H.; Merz, B. Assessing the Probability of Large-Scale Flood Loss Events: A Case Study for the River Rhine, Germany. *J. Flood Risk Manag.* **2015**, *8*, 247–262. [CrossRef]

14. Winter, B.; Schneeberger, K.; Huttenlau, M.; Stötter, J. Sources of Uncertainty in a Probabilistic Flood Risk Model. *Nat. Hazards* **2018**, *91*, 431–446. [CrossRef]
15. Quesada-Román, A.; Ballesteros-Cánovas, J.A.; Granados-Bolaños, S.; Birkel, C.; Stoffel, M. Improving Regional Flood Risk Assessment Using Flood Frequency and Dendrogeomorphic Analyses in Mountain Catchments Impacted by Tropical Cyclones. *Geomorphology* **2022**, *396*, 108000. [CrossRef]
16. Quesada-Román, A.; Villalobos-Chacón, A. Flash Flood Impacts of Hurricane Otto and Hydrometeorological Risk Mapping in Costa Rica. *Geogr. Tidsskr.-Danish J. Geogr.* **2020**, *120*, 142–155. [CrossRef]
17. Pinos, J.; Orellana, D.; Timbe, L. Assessment of Microscale Economic Flood Losses in Urban and Agricultural Areas: Case Study of the Santa Bárbara River, Ecuador. *Nat. Hazards* **2020**, *103*, 2323–2337. [CrossRef]
18. Zambri, A. DBKL Giat Tangani Limpahan Air Hujan 2020. Available online: https://www.wilayahku.com.my/dbkl-giat-tangani-limpahan-air-hujan/ (accessed on 10 June 2022).
19. Department of Irrigation and Drainage (DID). *Laporan Banjir Tahunan*; Department of Irrigation and Drainage (DID): Kuala Lumpur, Malaysia, 2010–2020.
20. de Moel, H.; Jongman, B.; Kreibich, H.; Merz, B.; Penning-Rowsell, E.; Ward, P.J. Flood Risk Assessments at Different Spatial Scales. *Mitig. Adapt. Strateg. Glob. Chang.* **2015**, *20*, 865–890. [CrossRef]
21. Murnane, R.; Simpson, A.; Jongman, B. Understanding Risk: What Makes a Risk Assessment Successful? *Int. J. Disaster Resil. Built Environ.* **2016**, *7*, 186–200. [CrossRef]
22. Zhou, Q.; Mikkelsen, P.S.; Halsnæs, K.; Arnbjerg-Nielsen, K. Framework for Economic Pluvial Flood Risk Assessment Considering Climate Change Effects and Adaptation Benefits. *J. Hydrol.* **2012**, *414–415*, 539–549. [CrossRef]
23. Li, J.; Zhao, Y.; Bates, P.; Neal, J.; Tooth, S.; Hawker, L.; Maffei, C. Digital Elevation Models for Topographic Characterisation and Flood Flow Modelling along Low-Gradient, Terminal Dryland Rivers: A Comparison of Spaceborne Datasets for the Río Colorado, Bolivia. *J. Hydrol.* **2020**. [CrossRef]
24. Takaku, J.; Tadono, T.; Tsutsui, K.; Ichikawa, M. Validation of "AW3D" global dsm generated from alos prism. *ISPRS Ann. Photogramm. Remote Sens. Spat. Inf. Sci.* **2016**, *III–4*, 25–31. [CrossRef]
25. Takaku, J.; Tadono, T.; Tsutsui, K. Generation of High Resolution Global DSM from ALOS PRISM. *Int. Arch. Photogramm. Remote Sens. Spat. Inf. Sci.* **2014**, *XL–4*, 243–248. [CrossRef]
26. Alaska Satellite Facility Distributed Active Archive Centre. ALOS PALSAR RTC Radiometric Terrain Corrected High-Res 2014. Available online: https://search.asf.alaska.edu/#/ (accessed on 22 June 2020).
27. Earth Resources Observation And Science (EROS) Center Shuttle Radar Topography Mission ({Srtm}) 1 Arc-Second Global 2017. Available online: https://earthexplorer.usgs.gov/ (accessed on 22 June 2020).
28. Cook, A.; Merwade, V. Effect of Topographic Data, Geometric Configuration and Modeling Approach on Flood Inundation Mapping. *J. Hydrol.* **2009**, *377*, 131–142. [CrossRef]
29. Prakash, M.; Rothauge, K.; Cleary, P.W. Modelling the Impact of Dam Failure Scenarios on Flood Inundation Using SPH. *Appl. Math. Model.* **2014**, *38*, 5515–5534. [CrossRef]
30. Yan, K.; Baldassarre, G.; Di Solomatine, D.P. Exploring the Potential of SRTM Topographic Data for Flood Inundation Modelling under Uncertainty. *J. Hydroinf.* **2013**, *15*, 849–861. [CrossRef]
31. Muthusamy, M.; Casado, M.R.; Butler, D.; Leinster, P. Understanding the Effects of Digital Elevation Model Resolution in Urban Fluvial Flood Modelling. *J. Hydrol.* **2021**, *596*. [CrossRef]
32. Saksena, S. Investigating the Role of DEM Resolution and Accuracy on Flood Inundation Mapping. In Proceedings of the World Environmental and Water Resources Congress 2015, Austin, TX, USA, 15 May 2015; American Society of Civil Engineers: Reston, VA, USA, 2015; pp. 2236–2243.
33. Kuala Lumpur City Hall. *Cadangan Menyediakan Pelan Induk (Master Plan) Untuk Sistem Saliran Dan Pengurusan Air Hujan Bagi Bandaraya Kuala Lumpur*; Kuala Lumpur City Hall: Kuala Lumpur, Malaysia, 2015.
34. Chow, V. *Te Open-Channel Hydraulics*; McGraw-Hill Book Company: New York, NY, USA, 1959.
35. Curtis, J. Manning's n Values for Various Land Covers. To Use for Dam Breach Analyses by NRCS in Kansas. 2016, pp. 1–2. Available online: https://rashms.com/wp-content/uploads/2021/01/Mannings-n-values-NLCD-NRCS.pdf (accessed on 8 April 2020).
36. Brunner, G.W. HEC-RAS River Analysis System, 2D Modeling User's Manual Version 5.0. 2016, pp. 1–171. Available online: https://www.hec.usace.army.mil/software/hec-ras/documentation/HEC-RAS%205.0%202D%20Modeling%20Users%20Manual.pdf (accessed on 31 May 2020).
37. Werner, M.G.F. Impact of Grid Size in GIS Based Flood Extent Mapping Using a 1D Flow Model. *Phys. Chem. Earth, Part B Hydrol. Ocean. Atmos.* **2001**, *26*, 517–522. [CrossRef]
38. Horritt, M.S.; Bates, P.D. Effects of Spatial Resolution on a Raster Based Model of Flood Flow. *J. Hydrol.* **2001**, *253*, 239–249. [CrossRef]
39. Bates, P.; De Roo, A.P. A Simple Raster-Based Model for Flood Inundation Simulation. *J. Hydrol.* **2000**, *236*, 54–77. [CrossRef]
40. Ghimire, E. Evaluation of One-Dimensional and Two-Dimensional HEC-RAS Models for Flood Travel Time Prediction and Damage Assessment Using HAZUS-MH: A Case Study of Grand River, Ohio. Master's Thesis, Youngstown State University, Youngstown, OH, USA, 2019.

41. Casulli, V. A High-Resolution Wetting and Drying Algorithm for Free-Surface Hydrodynamics. *Int. J. Numer. Methods Fluids* **2009**, *60*, 391–408. [CrossRef]
42. Martínez-Gomariz, E.; Forero-Ortiz, E.; Russo, B.; Locatelli, L.; Guerrero-Hidalga, M.; Yubero, D.; Castan, S. A Novel Expert Opinion-Based Approach to Compute Estimations of Flood Damage to Property in Dense Urban Environments. Barcelona Case Study. *J. Hydrol.* **2021**, *598*, 126244. [CrossRef]
43. Notaro, V.; De Marchis, M.; Fontanazza, C.M.; La Loggia, G.; Puleo, V.; Freni, G. The Effect of Damage Functions on Urban Flood Damage Appraisal. *Procedia Eng.* **2014**, *70*, 1251–1260. [CrossRef]
44. Rehan, B.M. An Innovative Micro-Scale Approach for Vulnerability and Flood Risk Assessment with the Application to Property-Level Protection Adoptions. *Nat. Hazards* **2018**, *91*, 1039–1057. [CrossRef]
45. Romali, N.S.; Yusop, Z. Flood Damage and Risk Assessment for Urban Area in Malaysia. *Hydrol. Res.* **2021**, *52*, 142–159. [CrossRef]
46. Wagenaar, D.J.; Dahm, R.J.; Diermanse, F.L.M.; Dias, W.P.S.; Dissanayake, D.M.S.S.; Vajja, H.P.; Gehrels, J.C.; Bouwer, L.M. Evaluating Adaptation Measures for Reducing Flood Risk: A Case Study in the City of Colombo, Sri Lanka. *Int. J. Disaster Risk Reduct.* **2019**, *37*, 101162. [CrossRef]
47. Wang, H.; Zhou, J.; Tang, Y.; Liu, Z.; Kang, A.; Chen, B. Flood Economic Assessment of Structural Measure Based on Integrated Flood Risk Management: A Case Study in Beijing. *J. Environ. Manage.* **2021**, *280*, 111701. [CrossRef] [PubMed]
48. Freni, G.; La Loggia, G.; Notaro, V. Uncertainty in Urban Flood Damage Assessment Due to Urban Drainage Modelling and Depth-Damage Curve Estimation. *Water Sci. Technol.* **2010**, *61*, 2979–2993. [CrossRef] [PubMed]
49. Department of Irrigation and Drainage Malaysia (DID). *Updating of Condition of Flooding and Flood Damage Assessment in Malaysia*; National Flood Forecasting and Warning Centre (PRABN): Kuala Lumpur, Malaysia, 2012; Volume 2.
50. Miller, J.; Kaelin, A.; Binti, B.; Rehan, M.; Sayers, P.; Davies, H.; Stewart, L. *National Exposure & Vulnerability Data and Methods for the Malaysian Peninsula*; Centre of Ecology and Hydrology: Wallingford, UK, 2020.
51. Banjara, S.; Acharya, T.R.; Deuja, S.; Thapa, S. Flood Risk Mapping of Upper Bagmati Basin. Bachelor's Thesis, Kathmandu University, Dhulikhel, Nepal, 2011.
52. Pappenberger, F.; Frodsham, K.; Beven, K.; Romanowicz, R.; Matgen, P. Fuzzy Set Approach to Calibrating Distributed Flood Inundation Models Using Remote Sensing Observations. *Hydrol. Earth Syst. Sci.* **2007**, *11*, 739–752. [CrossRef]
53. Zhang, Y. Using LiDAR-DEM Based Rapid Flood Inundation Modelling Framework to Map Floodplain Inundation Extent and Depth. *J. Geogr. Sci.* **2020**, *30*, 1649–1663. [CrossRef]
54. Xu, K.; Fang, J.; Fang, Y.; Sun, Q.; Wu, C.; Liu, M. The Importance of Digital Elevation Model Selection in Flood Simulation and a Proposed Method to Reduce DEM Errors: A Case Study in Shanghai. *Int. J. Disaster Risk Sci.* **2021**, *12*, 890–902. [CrossRef]
55. Garrote, J. Free Global DEMs and Flood Modelling—A Comparison Analysis for the January 2015 Flooding Event in Mocuba City (Mozambique). *Water* **2022**, *14*, 176. [CrossRef]
56. Hsu, Y.C.; Prinsen, G.; Bouaziz, L.; Lin, Y.J.; Dahm, R. An Investigation of DEM Resolution Influence on Flood Inundation Simulation. *Procedia Eng.* **2016**, *154*, 826–834. [CrossRef]
57. Saksena, S.; Merwade, V. Incorporating the Effect of DEM Resolution and Accuracy for Improved Flood Inundation Mapping. *J. Hydrol.* **2015**, *530*, 180–194. [CrossRef]
58. Sanders, B.F. Evaluation of On-Line DEMs for Flood Inundation Modeling. *Adv. Water Resour.* **2007**, *30*, 1831–1843. [CrossRef]
59. Yan, K.; Di Baldassarre, G.; Solomatine, D.P.; Schumann, G.J.P. A Review of Low-Cost Space-Borne Data for Flood Modelling: Topography, Flood Extent and Water Level. *Hydrol. Process.* **2015**, *29*, 3368–3387. [CrossRef]
60. Nafari, R.H. Flood Damage Assessment in Urban Areas. Ph.D. Thesis, University of Melbourne, Melbourne, Australia, 2018.
61. Vozinaki, A.-E.K.; Karatzas, G.P.; Sibetheros, I.A.; Varouchakis, E.A. An Agricultural Flash Flood Loss Estimation Methodology: The Case Study of the Koiliaris Basin (Greece), February 2003 Flood. *Nat. Hazards* **2015**, *79*, 899–920. [CrossRef]
62. Zahari, R.K.; Ariffin, R.N.R. Risk Communications: Flood-Prone Communities of Kuala Lumpur. *Procedia Environ. Sci.* **2013**, *17*, 880–888. [CrossRef]
63. Ward, P.J.; de Moel, H.; Aerts, J.C.J.H. How Are Flood Risk Estimates Affected by the Choice of Return-Periods? *Nat. Hazards Earth Syst. Sci.* **2011**, *11*, 3181–3195. [CrossRef]
64. Hawker, L.; Rougier, J.; Neal, J.; Bates, P.; Archer, L.; Yamazaki, D. Implications of Simulating Global Digital Elevation Models for Flood Inundation Studies. *Water Resour. Res.* **2018**, *54*, 7910–7928. [CrossRef]